p·s·s
physica status solidi **a**
www.pss-a.com
applications and materials science

Silicon carbide nanolayers as a solar cell constituent

V. Zakhvalinskii[1], E. Piliuk[1], I. Goncharov[1], A. Simashkevich*,[2], D. Sherban[2], L. Bruc[2], N. Curmei[2], and M. Rusu[2,3]

[1] State University of Belgorod, 85, Pobedy str., 308015 Belgorod, Russia
[2] Institute of Applied Physics, 5 Academiei str, 2028 Chisinau, Republic of Moldova
[3] Institut für Heterogene Materialsysteme, Helmholtz-Zentrum Berlin für Materialien und Energie GmbH, Lise-Meitner Campus, Hahn-Meitner-Platz 1, 14109 Berlin, Germany

* Corresponding author: e-mail alexeisimashkevich@hotmail.com, Phone: +373 22 738054, Fax: +373 22 738149

Thin films of predominantly amorphous n-type SiC were prepared by non-reactive magnetron sputtering in an Ar atmosphere. A previously synthesized SiC was used as a solid-state target. Deposition was carried out on a cold substrate of p-type Si (100) with a resistivity of $2\,\Omega\mathrm{cm}$. The Raman spectrum shows a dominant band at $982\,\mathrm{cm}^{-1}$, i.e., in the spectral region characteristic for SiC. It was found that the root mean square roughness varies from about 0.3 nm to 9.0 nm when the film thickness changes from about 2 nm to 56 nm, respectively. Transmission electron microscopy studies showed that SiC thin films consist predominantly of an amorphous phase with inclusions of very fine nanocrystallites. A heterostructure consisting of a p-type Si (100) and a layer of predominantly amorphous n-type SiC was fabricated and studied. The investigation of its electrical and photoelectric properties shows that the entire space charge region is located in Si. This is in addition confirmed by the spectral dependence of the p-Si/n-SiC photosensitivity. The barrier height at the p-Si/n-SiC interface estimated from dark $I\text{–}V$ characteristics is of the order of 0.9–1.0 eV. Load $I\text{–}V$ characteristics of p-Si/n-SiC-nanolayer solar cells demonstrate under standard AM1.5 illumination conditions a conversion efficiency of 7.22%.

1 Introduction Despite the development of new generations of solar cells (SCs) based on new principles and technologies, silicon remains the basic material for the production of photovoltaic (PV) devices. However, broader terrestrial application of Si-based PV cells is still limited, since the cost of electricity generated by these devices is still too high. Therefore, there is a wide search for new opportunities to reduce this cost by the use of new materials and structures for the production of silicon based devices. In particular, good perspectives have SC heterostructures based on SiC semiconductor which have already achieved an efficiency exceeding 15% [1–4]. These devices are designed to operate at an increased level of incident radiation and high temperature. However, the constraint is the cost of SiC in meeting the requirements of the electronics industry which averages at least $ 100 per 1 sq. inch [5]. The difficulties for the application of SiC in electronics are related in addition to the SiC polymorphism: the amount of crystalline modifications of silicon carbide is more than 200. Crystalline layered superstructure SiC is built from elementary layers of three types. The periodicity of elementary layers varies from tens of angstroms to tens of nanometres. The n-type conductivity of SiC is usually caused by doping with nitrogen or phosphorus, while the p-type conductivity is determined by aluminium, boron, gallium, or beryllium impurities [6].

The problem of increased consumption of SiC can be solved by the use of amorphous SiC (a-SiC) and nano-crystalline SiC (nc-SiC). The most often used methods for the preparation of a-SiC:H represent different modifications of the chemical vapor deposition (CVD) method such as hot wire chemical vapor deposition (HWCVD) and hot filament CVD (HFCVD) known also as catalytic chemical vapor deposition (Cat-CVD). For the preparation of the a-SiC thin films by these methods, environmentally harmful silane (SiH_4), propane (C_3H_8), and phosphine (PH_3) are used [7, 8].

The aim of this study is to develop environmentally friendly preparation methods for SiC thin films and demonstrate competitive solar cell devices. In this work,

Phys. Status Solidi A 212, No. 1 (2015)

185

SiC-nanolayers were prepared by using an RF-magnetron sputtering. p-Si/n-SiC solar cells with an efficiency of 7.22% under AM1.5 standard test conditions are demonstrated.

2 Preparation of SiC nanolayers SiC thin films were prepared by the method of high-frequency non-reactive magnetron sputtering in an Ar atmosphere using an Ukrro-spribor VN-2000 setup. A previously synthesized silicon carbide was used as a solid-state target. The depositions were carried out on a cold substrate of p-Si (100) with a resistivity of 2 Ωcm. The layer of silicon oxide was removed from Si substrate by chemical etching in HF before the SiC thin film deposition. Three series of samples with different n-SiC thin film thicknesses of about 2 nm (series 1), 6 nm (series 2), and 56 nm (series 3) have been deposited on p-Si substrates.

3 Characterization of SiC nanolayers The composition of deposited layers was characterized by Raman Spectroscopy (RS) techniques using co-focal nanometric resolution Omega Scope AIST-NT Raman microscope excited with an 532 nm Ar^+ laser. The Raman spectrum of the obtained layers is presented in Fig. 1. The spectra show a dominant band at 982 cm^{-1}, i.e., in the spectral region close to the frequency of the modes characteristic of SiC [9].

The successful application of multilayer structures depends on the ability to control the morphology and structure at each interface. The morphology features of SiC thin films was studied by tapping-mode atomic force microscopy (AFM) (NTEGRA Aura, NT-MDT) in a controlled atmosphere or low vacuum. The quantitative analysis of the obtained AFM data has been performed using the roughness analysis method described in Ref. [10]. Computational processing of the AFM images was performed using the software package «Image Analysis P9» (NT-MDT).

The thin film thicknesses were determined from the step height at the edge of the SiC films. An example is shown in Fig. 2.
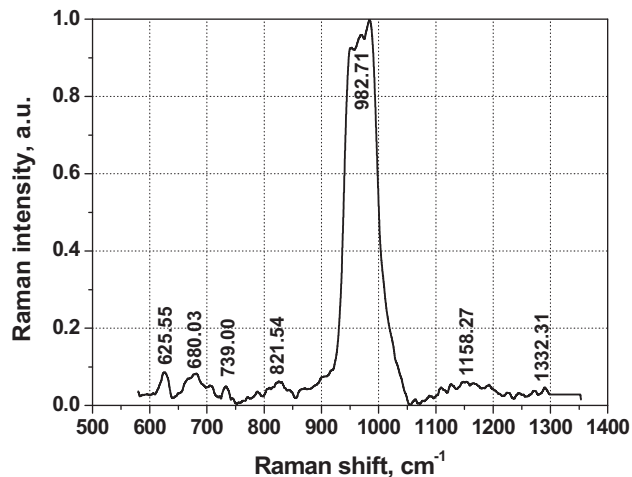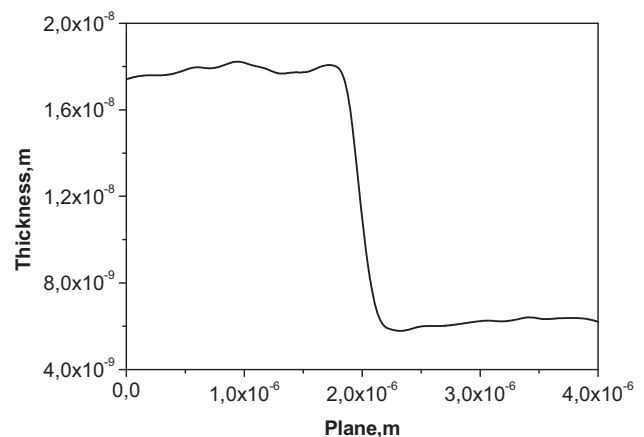

Figure 2 SiC layer profile at the film edge determined by AFM method.

The morphology features of SiC thin films were investigated as a function of the layer thickness. Figure 3 demonstrates the evolution of the surface morphology of SiC films with thicknesses between 2 nm and 56 nm (Series 1–3). As can be seen from Fig. 3, the average height of the surface features varies depending on the film thickness from 1–2 nm (Fig. 3a) to 3–5 nm (Fig. 3b) and 25–35 nm (Fig. 3c) when the film thickness changes from 2 nm to 6 nm and 56 nm, respectively.

The lateral dimensions of those elements are of the order of tens of nanometres.

The results of the scaling analysis applied to layers of Series 1–3 is summarized in the following. The global roughness scaling parameters were extracted from the AFM scans. A 2D autocorrelation function was applied to the AFM images and provided a means for identifying the anisotropic average island sizes. Figure 4 shows height distribution histograms of the surface elements for SiC nanolayer samples displayed in Fig. 3.

The results of quantitative analysis of the obtained AFM data for each nanolayer series are reported in Table 1. It shows the so called S-parameters or 3D parameters that characterize the surface structure, given that the surface is three-dimensional [11]. As a result of the data analysis it was found that the root mean square roughness (RMS) S_q increases from 0.3 nm to about 9 nm when the film thickness increases from approximately 2 nm to 56 nm, respectively. The surface area ratio, S_{dr}, increases with the film thickness as well. However, the coefficient of asymmetry, S_{sk}, that describes the shape of the distribution function of the amplitude, i.e., the symmetry of the scatter profile relative to the mean value, varies differently. For the films with a thickness of 2 nm and 56 nm, this coefficient is approximately equal to zero. For the films with a thickness of 15 nm, the factor S_{sk} is equal to 0.7, which shows the asymmetry of the surface profile.

The structure of the SiC thin films is investigated by electron diffraction obtained in a JEOL Ltd. JEM 2100
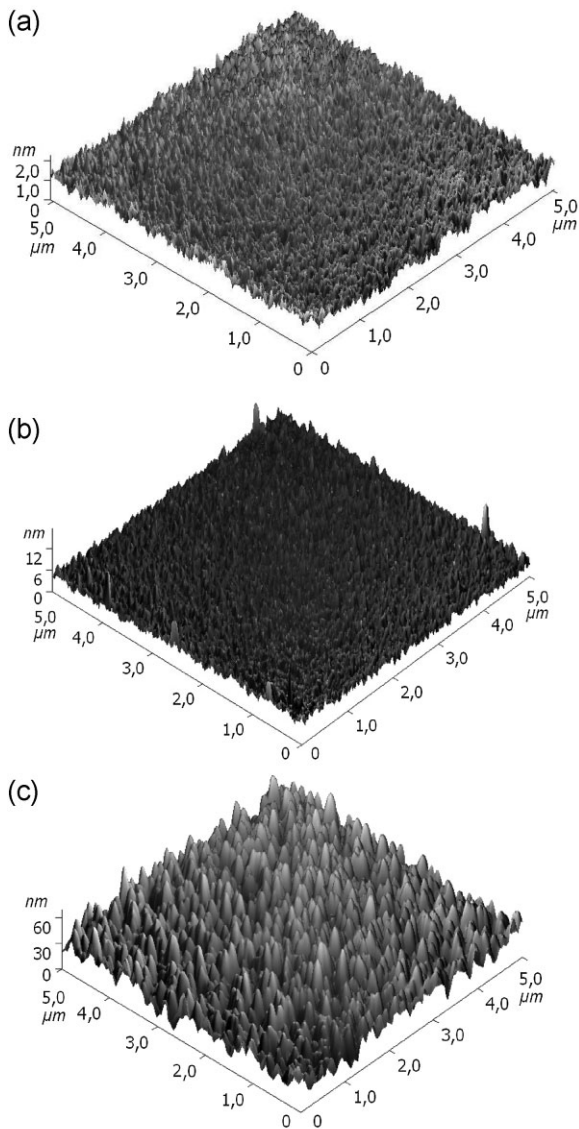

Figure 1 Raman spectrum of a SiC nanolayer prepared by high-frequency non-reactive magnetron sputtering in Ar.

(a)

(a)

(b)

(b)

(c)

(c)

Figure 3 Surface morphology of SiC thin films with different thicknesses measured by AFM.

Figure 4 Height distribution histograms of SiC nanolayers corresponding to Fig. 3a–c.

transmission electron microscope. A diffraction pattern of a SiC thin film grown on a Si (100) substrate is shown in Fig. 5a. Diffuse diffraction rings with some blurred spots are observed. Diffuse diffraction rings are indicative for an amorphous phase, whilst the blurred spots suggest the presence of a low crystallinity phase. In addition, the presence of diffraction rings shows the absence of the dominant orientation of the SiC thin film deposited on Si (100) substrate. From Fig. 5b the islet-like structure of the investigated SiC thin film is clearly visible. Thus, SiC thin films consist predominantly of amorphous islets with inclusions of very fine nanocrystallites.

These results correlate well with the data obtained by atomic force microscopy and confirm the fine structure of the film.
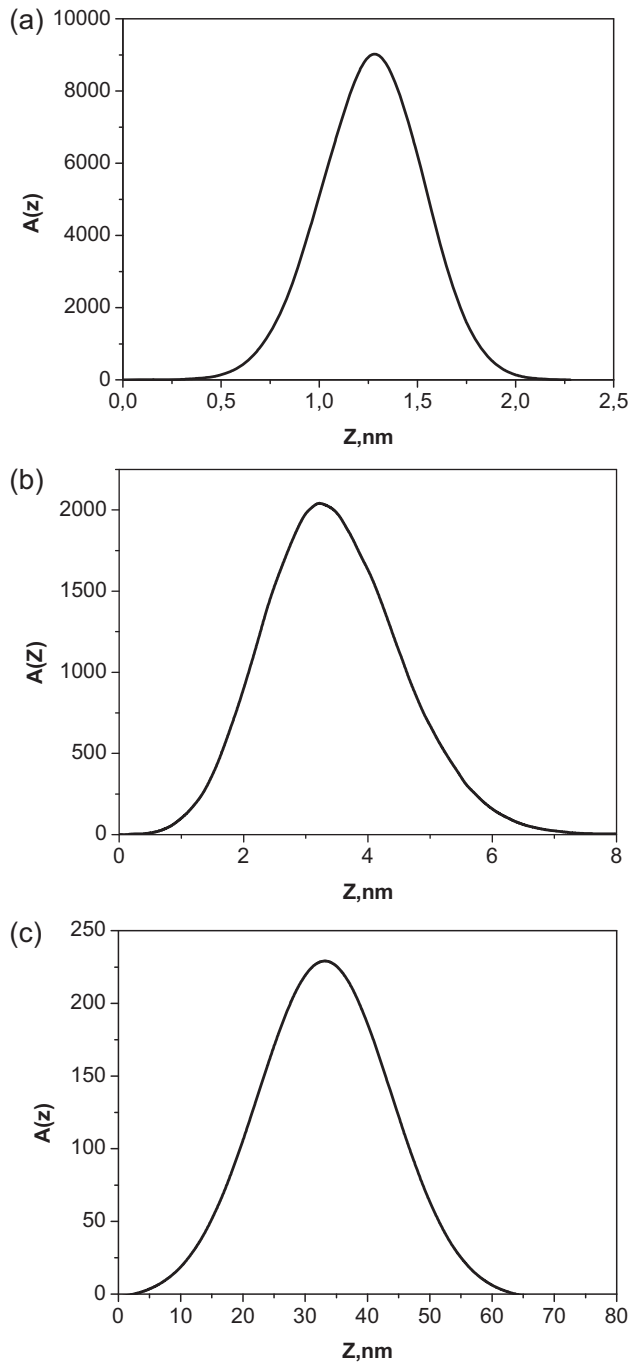
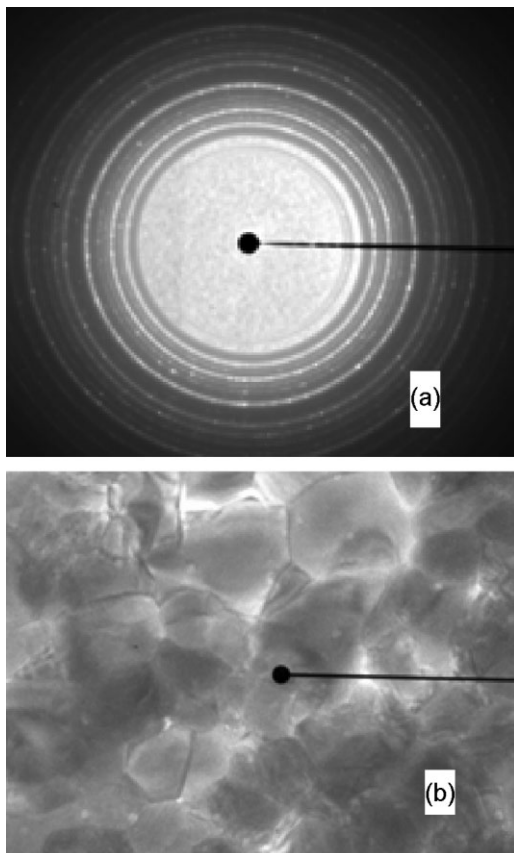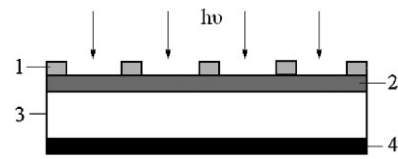**4 p-Si/n-SiC-nanolayer photovoltaic cell: Preparation and characterization** We have prepared a heterojunction photovoltaic cell consisting of a substrate of p-type Si covered by a layer of predominantly amorphous n-type SiC. The Si substrate was specially treated with chemical etchants before the SiC layer deposition. The best results have been achieved with SiC layers with the thickness of 10 nm. An Ag grid has been deposited as top electrode for

Table 1 Statistical analysis of the morphology of SiC nanolayers with a sampling area of $25\,\mu m^2$.

| parameters	serie 1	serie 2	serie 3
S_y, peak-to-peak (nm)	2.3	15.2	56.2
S_z, ten point height (nm)	1.2	13.1	28.0
average height (nm)	1.3	3.6	27.4
S_a, average roughness (nm)	0.2	0.9	7.3
S_q, RMS (nm)	0.3	1.1	9.0
S_{sk}, surface skewness	−0.1	0.7	0.1
S_{ku}, coefficient of kurtosis	3	5.7	2.8
S_{3A}, surface area (μm^2)	25.01	25.1	25.9
S_{dr}, surface area ratio (%)	0.01	0.2	3.3

silicon carbide thin film. A continuous Cu layer has been deposited as back electrode. The cross-section schematic of the solar cell device is shown in Fig. 6.

The dark *I–V* characteristic of the elaborated p-Si/n-SiC solar cell is shown in Fig. 7. The barrier height at the Si/SiC interface estimated from dark *I–V* measurements performed at different temperatures is of the order of 0.9–1.0 eV. These values are much higher than the half of Si band gap. Therefore, we conclude that the physical p–n junction is

Figure 6 Cross-section schematic of the p-Si/n-SiC solar cell: 1 front grid (Ag), 2 n-SiC amorphous layer, 3 single-crystal p-Si substrate, 4 back contact (Cu).
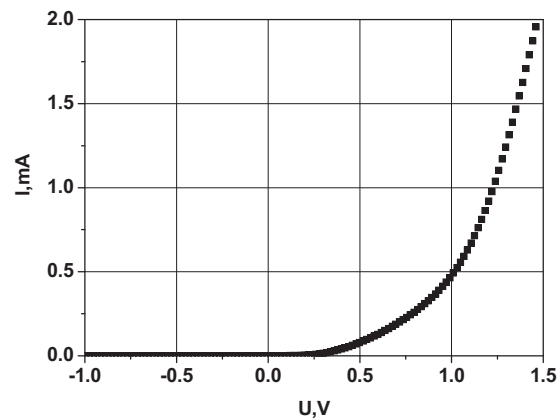
Figure 7 Dark current–voltage characteristic of a p-Si/n-SiC solar cell.

located in the Si substrate near the Si/SiC interface; the entire space charge region, where the light absorption takes place and charge carriers are generated and separated, is located in Si. This fact is in addition confirmed by the spectral dependence of the Si/SiC photosensitivity in Fig. 8 which entirely matches the respective characteristic of Si solar cells.

The measurements of the load current–voltage characteristics of the as-prepared p-Si/n-SiC solar cells and the determination of their photoelectrical parameters have been carried out under standard AM1.5 conditions (1000 W/m^2, 25 °C) with an ST-1000 solar simulator.

Figure 5 (a) Diffraction pattern and (b) cross-section TEM image of a SiC thin film.
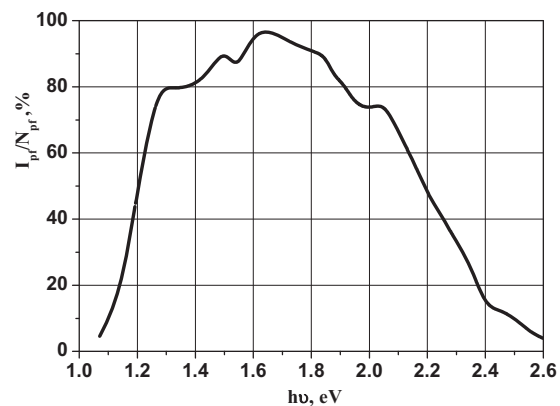
Figure 8 Spectral dependence of the p-Si/n-SiC solar cell photosensitivity.
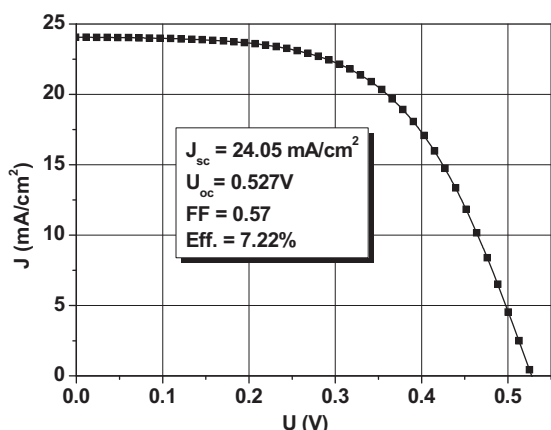
Figure 9 *I–V* load characteristic of a p-Si/n-SiC solar cell.

A *I–V* load characteristic of a Si/SiC solar cell is presented in Fig. 9. The short-circuit current density is 24.05 mA/cm^2, the open-circuit voltage is 0.527 V and the fill factor is 57%.

The solar energy conversion efficiency of the elaborated solar cell device reaches 7.22%.

5 Conclusions Thin films of n-type SiC were prepared by non-reactive magnetron sputtering in an Ar atmosphere. TEM studies showed that SiC thin films consist predominantly of amorphous islets and nanocrystalline inclusions. The control of the SiC thin film thickness and the study of the surface morphology were performed by the tapping mode atomic force microscopy under a controlled atmosphere or low vacuum. The computational processing of the AFM images revealed that the mean-square roughness, S_q, increases from 0.3 nm to 9 nm when the film thickness increases from 2 nm to 56 nm, respectively. However, the asymmetry coefficient for the films with thicknesses of 8 nm and 40 nm is nearly zero, while for the films with the thickness of 15 nm is different from zero, thus indicating the asymmetry of the profile of the film surface.

A heterostructure Ag/n-SiC/p-Si/Cu solar cell device was demonstrated. It was found from electrical and photoelectric measurements that the entire space charge region is located in Si. The barrier height at the Si/SiC interface estimated from dark *I–V* measurements is of the order of 0.9–1.0 eV. The spectral dependence of the Si/SiC photosensitivity entirely corresponds to the respective characteristic of the Si solar cells. Load *I–V* characteristics of the elaborated solar cell under standard AM1.5 test conditions demonstrate a conversion efficiency of 7.22%. This encouraging result shows that the proposed approach can be considered as a promising low-temperature innovative technology for fabrication of cost-effective solar cells.

References

[1] A. Solangi, and M. I. Chaudry, Springer Proc. Phys. **71**, 362 (1992).

[2] C. Banerjee, K. Haga, S. Miyajima, A. Yamada, and M. Konagai, Jpn. J. Appl. Phys. **46**, 1 (2007).

[3] Y. Matsumoto, G. Hirata, H. Takakura, H. Okamoto, and Y. Hamakawa, J. Appl. Phys. **67**, 6538 (1990).

[4] X. Wu, X. Chen, L. Sun, S. Mao, and Z. Fu, J. Semicond. **31**, 103002-1 (2010).

[5] V. Luchinin and Iu. Tairov, Contemp. Electron. **7**, 12 (2009) (in Russian).

[6] H. Morkoç, S. Strite, G. B. Gao, M. E. Lin, B. Sverdlov, and M. Burns, J. Appl. Phys. **76**, 1364 (1994).

[7] Y. Tawada and H. Yamagishi, Sol. Energy Mater. Sol. Cells **66**, 95 (2001).

[8] Y. Hamakawa, J. Physique **42**, C4-1131 (1981).

[9] J. Wasyluk, T. S. Perova, S. A. Kukushkin, A. V. Osipov, N. A. Feoktistov, and S. A. Grudinkin, Mater. Scie. Forum **645-648**, 359 (2010).

[10] M. Raposo, Q. Ferreira, and P. Ribeiro, in: Modern Research and Education Topics in Microscopy, edited by A. Medez-Vilas, and J. Diaz (Badajoz, Spain, FORMATEX, 2007). p 758.

[11] L. Blunt, and X. Jiang, Advanced Techniques for Assessment Surface Topography: Development of a Basis for 3D Surface Texture Standards "Surfstand" (Butterworth-Heinemann, London, 2003), p 340.